

Precipitation chemistry and deposition at a high-elevation site in the Pacific Northwest United States (1989–2015)



Anne M. Johansen^{a,*}, Clint Duncan^a, Ashleen Reddy^a, Naomi Swain^a, Mari Sorey^a, Annika Nieber^a, James Agren^a, Matt Lenington^a, David Bolstad^a, Barbara Samora^b, Rebecca Lofgren^b

^a Chemistry Department, Central Washington University, 400 E. University Way, Ellensburg, WA, USA

^b Mount Rainier National Park, 55210 238th Avenue East, Ashford, WA, USA

ARTICLE INFO

Keywords:

Acid deposition
Nitrate
Ammonium
High-elevation
Long-term
Mount rainier national park

ABSTRACT

Emissions from fuel combustion and agricultural activities contribute significantly to the continuous atmospheric entrainment of pollutants into protected and vulnerable ecosystems where long-term monitoring is often a challenge. Here, results are presented from a 26-year study (1989–2015) of wet precipitation collected at Paradise Station (1654 m above sea level), Mount Rainier National Park, Washington, USA. Weekly samples were analyzed for pH, conductivity and major anions and cations. While precipitation concentrations for sulfate, nitrate, protons and conductivity peaked in the early 2000s, overall trends decreased by 54%, 46%, 41%, and 37%, respectively. Associated pH values increased from 5.2 to 5.6, and were largely controlled by non-sea-salt contributions of sulfate and neutralizing calcium, potassium and magnesium. Between 1999 and 2015, nitrogen (N) deposition rates from ammonium increased by a factor of 3.6, from 0.27 to 0.96 kg N ha⁻¹ yr⁻¹ ($p = 0.02$), while nitrate deposition did not change statistically (0.91–0.74 kg N ha⁻¹ yr⁻¹, $p = 0.30$). Combined, these N sources are reaching reported critical loads of 2.0 kg N ha⁻¹ yr⁻¹. Results indicate that emission regulations focused on stationary sources have effectively decreased apparent acid precipitation, however, increased nitrogen deposition from ammonium may lead to further fertilization and acidification of delicate soils and waters. Continued long-term monitoring is thus imperative to track continued anthropogenic inputs to vulnerable ecosystems.

1. Introduction

Precipitation chemistry and deposition rates are important factors in understanding and predicting the effects of anthropogenic atmospheric emissions on ecosystems. Of particular concern is the deposition of nitrogen (N) to protected areas where it may be a limiting nutrient to biota thus leading to issues including eutrophication and decreased biodiversity (Baron, 2006; Benedict et al., 2013; Ellis et al., 2013; Fenn et al., 2003; Pardo et al., 2010). Furthermore, excess N and sulfur (S) deposition can cause acidification of aquatic systems and soils, especially in waters of low alkalinity or acid-neutralization capacity (ANC) such as at high elevation sites (Fenn et al., 2012; Greaver et al., 2012; Vet et al., 2014). To protect these areas in U.S. National Parks, the National Park Service (NPS) Organic Act mandated that natural resources are to be left “unimpaired for the enjoyment of future generations” (National Park Service, 2006). In

addition, the Clean Air Act provides special protection for Class I air quality areas including national parks larger than 6000 acres and national wilderness areas larger than 5000 acres. Mount Rainier National Park is one of 48 of the National Park System with Class I areas. Because atmospheric transport and deposition of pollutants to these regions is unavoidable it is imperative to monitor over long timeframes atmospheric components, sources, deposition, and trends. In addition, reductions in pollution in Class I parks will also improve air quality in adjacent parks and in the surrounding region. Here we present precipitation chemistry data collected between 1989 and 2015 at a high-elevation site at Paradise located within Mount Rainier National Park, WA. Because of the practical challenges of sampling at high elevation, particularly during the snowy season, such long-term field observations are scarce and therefore valuable in determining the relationship between natural processes and perturbations brought about by human activities.

* Corresponding author.

E-mail addresses: johansea@cwu.edu (A.M. Johansen), duncancands@msn.com (C. Duncan), redya@cwu.edu (A. Reddy), beebekn7@gmail.com (N. Swain), tamarisorey@yahoo.com (M. Sorey), niebera@gmail.com (A. Nieber), jamesagren@gmail.com (J. Agren), matt.lenington123@gmail.com (M. Lenington), davidbolstad@gmail.com (D. Bolstad), bsamora@mashell.com (B. Samora), rebecca_a_lofgren@nps.gov (R. Lofgren).

<https://doi.org/10.1016/j.atmosenv.2019.05.021>

Received 7 February 2019; Received in revised form 7 May 2019; Accepted 11 May 2019

Available online 21 May 2019

1352-2310/© 2019 Elsevier Ltd. All rights reserved.

Anthropogenic inorganic N enters the atmosphere mainly from industry and high-temperature combustion of fossil and biomass fuels (as $\text{NO}_x = \text{NO} + \text{NO}_2$). In addition, agricultural activities including livestock production and fertilizer application are the main sources of atmospheric ammonia emission (NH_3) and a significant source of nitrous oxide (N_2O). Natural N emissions from soils, waters and lightning (as N_2O , NO and NH_3) are greatly surpassed in magnitude by emissions from said human activities, thus perturbing the natural N cycle (Fowler et al., 2013; Ghaly and Ramakrishnan, 2015; Hundey et al., 2016; Liu et al., 2013). Due to the use of catalytic converters and mandated regulations in certain regions, anthropogenic NO_x emission trends seem to be leveling out in the US, Europe, and China (Amann et al., 2013; Fenn et al., 2003; Gu et al., 2013; Vet et al., 2014). NH_3 emissions, however, have generally increased as a result of agricultural activities and livestock production (Amann et al., 2013; Lajtha and Jones, 2013). Anthropogenic S (as SO_2) stems mainly from the combustion of S containing fossil fuel (Amann et al., 2013). Controls in SO_2 emissions in both the US and Europe were first put in place in the 1960s and 1970s with subsequent amendments in the mid-1990s. These measures have led to generally declining SO_2 emissions since the mid-1970s, however, legacy impacts from continued long-term deposition and associated acidity are observed (Amann et al., 2013; Kaushal et al., 2013; Klimont et al., 2013; Smith et al., 2011; Sullivan et al., 2018). NO_x and SO_2 acidity stems from the generation of acidic protons (H^+) during oxidation to nitrate (NO_3^-) and sulfate (SO_4^{2-}), respectively, which have also leveled off, or decreased, in the US and Europe (e.g., (Lajtha and Jones, 2013; Lynch et al., 2000; Muri, 2013; Murray et al., 2013; Naftz et al., 2011; Vet et al., 2014)).

Emissions of NH_3 have increased for many areas of the U.S. (Pardo et al., 2011; Zhang et al., 2018). Ammonia effectively neutralizes acidity by acting as a base and forming ammonium (NH_4^+). This process leads to the precipitation of ammonium sulfate ($(\text{NH}_4)_2\text{SO}_4$) and ammonium nitrate (NH_4NO_3) salts that form particles, a.k.a., aerosols. The stoichiometry between these acids, bases and protons is complexified by the presence of other components in the aerosol phase that partake in acid-base equilibria and control precipitation pH. In particular, carbonates, hydroxides, and oxides, which stem from fly ash and dust are able to neutralize acidity. These bases can be tracked through the analysis of their respective cations, including Ca^{2+} , Mg^{2+} , and K^+ .

To better predict the impact of atmospheric deposition to a particular ecosystem critical loads (CL), or thresholds, are established that provide measures of N that the ecosystem can handle (Benedict et al., 2013; Clark et al., 2018; Geiser et al., 2011; Glavich and Geiser, 2008; Nanus et al., 2012; Pardo et al., 2010; M W Williams and Tonnessen, 2000). Soils, waters and biota can neutralize acid and take up N as a nutrient up to a certain limit, at which point the CL is reached and further acid deposition and nutrient addition causes significant degradation of important nutrients, stripping of soil, damaging of vegetation, and changes in biotic community structure and composition. High-elevation lakes can be particularly vulnerable to N input and acidification because they are oligotrophic, they receive more precipitation, are surrounded by exposed bedrock, and are low in mineral alkalinity due to low weathering rates of bedrock. Interestingly, in a study performed in Rocky Mountain National Park, it was established that N deposition was significantly higher at high-elevation (> 2500 m) compared to lower elevation National Atmospheric Deposition Program (NADP) sites: $2.5\text{--}3.5 \text{ kg ha}^{-1} \text{ yr}^{-1}$ vs. less than $2.5 \text{ kg ha}^{-1} \text{ yr}^{-1}$, respectively (M W Williams and Tonnessen, 2000). CLs for N deposition at Rocky Mountain National Park were established to vary between 1.5 and $7.1 \text{ kg ha}^{-1} \text{ yr}^{-1}$ depending on the ecosystem component (Baron, 2006; Fenn et al., 2013; Fenn et al., 2012; Geiser et al., 2011). Recent focus has been to determine analogous parameters for Washington State National Parks. While N deposition rates in summer 2008 at one lake in Olympic National Park varied from 0.6 to $2.4 \text{ kg ha}^{-1} \text{ yr}^{-1}$, the CL was estimated to be $1.0\text{--}1.2 \text{ kg ha}^{-1} \text{ yr}^{-1}$ (Sheibley et al., 2014). A more recent study performed on western mountain lakes estimated that a CL

of $2.0 \text{ kg N ha}^{-1} \text{ yr}^{-1}$ would avoid shifting plankton biomass limitation from N to P (J J Williams et al., 2017), while lowest CL, established for lichen for Northwestern Forested Mountains were $2.0\text{--}2.8 \text{ kg N ha}^{-1} \text{ yr}^{-1}$ (Clark et al., 2018).

NH_4^+ deposition has gained focus due to observed increases at high-elevation sites and elsewhere (Butler et al., 2016; Fakhraei et al., 2016; Sullivan et al., 2018). Although NH_4^+ in precipitation is a neutralizing agent due to its initial presence as NH_3 , once deposited onto soils it undergoes nitrification which is associated with the formation of 2 H^+ per NH_4^+ . Pardo et al. (2011) summarized that one or more CLs may be exceeded in most parks and wilderness areas.

The overarching goal of this study is to quantify magnitudes and long-term changes of precipitation chemistry and associated deposition of major ions to a high-elevation sensitive ecosystem. Weekly precipitation samples were collected, analyzed and compared to analogous data collected at a nearby, lower elevation site, as well as to general trends elsewhere.

2. Materials and methods

2.1. Site description

The Paradise collection site is located at the Mount Rainier Paradise Ranger Station, at 1654 m above sea level, within Mount Rainier National Park (Fig. S1). The NADP's National Trends Network (NTN) sites located in WA are Hoh (NADP ID: WA14), La Grande (WA21), Marblemount (WA19) and Tahoma Woods (WA99), where Tahoma Woods (424 m) is located just outside the Park boundary, 30 miles southeast of the Paradise Ranger Station, in Ashford, WA (see Fig. S1 for a map). The predominant wind direction at Paradise is from the West with sporadic winds from the West Northwest that may pick up potential pollutants from the Puget Sound Metropolitan Area (see Fig. S2 for wind roses). East winds are not uncommon during winter months when they are associated with the jet stream coming from the North, sweeping over inland Canada, eastern Washington and even Oregon before reaching Paradise (see Fig. S3 for representative 5-day air mass back trajectories). While the general provenance of all these air masses is from the North Pacific Ocean, they may contain regional agricultural and urban signatures.

2.2. Precipitation collection

As practically feasible, NTN sampling and analyses procedures were followed. However, due to the high volumes of snowfall, averaging 643 inches (53.6 feet or 16.3 m) per year based on data between 1920 and 2015, a wet-dry collector such as the one used at NADP sites (i.e., Aerochem Metrics Model 301 collector (ACM)) was not possible throughout all seasons and years.

Weekly collection of wet and dry deposition in the form of rain and snow commenced Jan. 25, 1989 and is ongoing. Data presented here includes samples collected up until June 3, 2015. Two longer data breaks exist due to sampling interruption: between May 1990 and November 1991, and October 2000 and May 2001. Up until October 2000, the ACM collector was used in the summers when possible (32% of sampling). Thereafter, collection was carried out with an open 5-gallon HDPE white plastic container placed on top of a 10-m collection tower at Paradise Station, Mount Rainier, removed from nearby vegetation and roads (see Fig. S4). The standard opening of 28.5-cm diameter was reduced during snowfall months by capping it with an inverted trimmed funnel of smaller opening to prevent bucket over-filling (see Fig. S4 right panel). Depending on the funnel used, the diameter of the opening varied between 12.8 and 16.0 cm (see SI for more details).

The sample interval most generally spanned one week, with exceptions due to reasons out of immediate control, such as road closures or bucket loss during heavy snow events. This resulted in 8810 sampling days and 1161 collected buckets over the indicated study period

between 1989 and 2015. Of the 1161 buckets, 31% (n = 366) were dry, did not contain enough sample to perform analyses, or were known to be contaminated. This number includes samples that were lost due to collector malfunction or technician error. Of the remaining 795 samples, 59 samples spanned a longer collection period than the planned 1-week (± 2 days). The 795 samples were chemically analyzed and further tested for robustness and completeness as described below.

2.3. Chemical and data analysis

Chemical analysis was performed in the accredited Central Washington University (CWU) Environmental Testing Laboratory. Inorganic anions (Cl^- , NO_3^- , SO_4^{2-}) were quantified by Ion Chromatography (IC) in anion mode using EPA Method 300.0. Determination of inorganic cations (Na^+ , NH_4^+ , K^+ , Mg^{2+} , Ca^{2+}) was accomplished by IC with EPA Method 300.7. Conductivity and pH were measured using a YSI 3200 Conductivity Meter and an Orion model 420A pH Meter (EPA Methods 120.1 and 150.1, respectively). Charge ratios were computed by adding the equivalent concentrations of all quantified positive ions, including H^+ from pH, and all quantified negative ions, and dividing the sum of positive by the sum of negative charges.

Every sample was checked against method detection limits (MDL) and subjected to ion balance (IB) and conductivity criteria (CC) following standard methods outlined in the SI. This process left n = 628 valid samples that were then corrected for evaporation and used to compute precipitation weighted quarterly average concentrations, similar as performed for NADP's NTN site samples (NADP, 2009).

To correct for evaporative losses due to the open bucket, observed sample concentrations (C_i) were corrected for the potential loss of water by multiplication with the ratio of collected precipitation volume (V) over the actual precipitation volumes ($V_{Mt.Rainier}$) as recorded at the co-located NOAA Paradise station (ID: USC00456898) or the nearby Natural Resources Conservation Snotel Site (AFSW1):

$$C_{i,corr} = \frac{C_i V}{V_{Mt.Rainier}} \quad (1)$$

When $V > V_{Mt.Rainier}$, NOAA, comparison was made with Snotel's precipitation amounts and its volume was used for $V_{Mt.Rainier}$ unless $V > V_{Mt.Rainier}$, Snotel, at which point $V_{Mt.Rainier} = V$. For pH, evaporation corrections for the concentration of protons was not applied. This was motivated by the fact that it is unlikely that the pH changes significantly as a result of evaporation in a proton-buffered system such as encountered in these environmental samples.

To obtain statistically more robust data, investigate seasonal differences, and compare with NTN sites, quarterly precipitation weighted average (PWA) concentrations were then computed analogously to NTN sites:

$$C_{i,corr,quarter} = \frac{\sum C_{i,corr} V_{Mt.Rainier}}{\sum V_{Mt.Rainier}} \quad (2)$$

Quarters are defined by season and as follows: winter = December–February, spring = March–May, summer = June–August, fall = September–November. Since winter begins with December of the previous year, the annual totals and means are offset by one month compared to typical annual values. Modified NADP completeness criteria were applied to these quarterly averages which resulted in a maximum number of quarterly averages of n = 81 (see SI for more details).

Deposition loads were computed for each quarter using the following equation:

$$DepLoad_{species,quarter} = C_{species,corr,quarter} \cdot Precip_{NOAA,quarter} \cdot \left(\frac{mol}{|z|} \cdot \frac{1}{10^6 \mu} \cdot \frac{1L}{10^3 cm^3} \cdot AM_{ion} \cdot \frac{1kg}{10^3 g} \cdot \frac{10^8 cm^2}{1ha} \right) \quad (3)$$

where $C_{species,corr,quarter}$ is the sample concentration expressed in $\mu\text{eq L}^{-1}$, z is the charge of the ion, $Precip_{NOAA,quarter}$ is the NOAA precipitation in cm and AM_{ion} is the atomic mass of the N or S in the respective ion (i.e., N for NO_3^- and NH_4^+ , and S for SO_4^{2-}). The Quarterly Deposition Load (QDL) is thus expressed in $\text{kg N ha}^{-1} \text{ quarter}^{-1}$ for NO_3^- and NH_4^+ , and in $\text{kg S ha}^{-1} \text{ quarter}^{-1}$ for SO_4^{2-} . For protons the QDL is expressed in $\text{keq H}^+ \text{ ha}^{-1} \text{ quarter}^{-1}$. Where appropriate, quarterly deposition loads are also expressed in $\text{meq m}^{-2} \text{ quarter}^{-1}$. To obtain more robust data for yearly deposition rates, seasonally averaged precipitation corrected quarterly data were averaged over 5-years for periods between 1989–1995 (6-years), 1996–2000, 2001–2005, 2006–2010, and 2011–2015. Individual yearly deposition estimates could not be computed due to data gaps in quarterly averages.

2.4. Statistical analysis

Precipitation time series are typically affected by three basic components: the underlying trend (T), seasonal variations (S) and random events (residual, R). The quarterly data set is a discrete-time stochastic process for which a multiplicative classical decomposition model (e.g., (Brockwell and Davis, 2016; Prema and Rao, 2015)) posits that for each quarter one can write:

$$C_{corr,quarter} = T_{quarter} \times S_{quarter} \times R_{quarter} \quad (4)$$

where $T_{quarter}$ is the linear trend component that captures how the concentration of a species changes slowly over longer time scales; $S_{quarter}$, is a seasonal component with period 4 that captures periodic changes in the mean behavior of the series, and the remaining term $R_{quarter}$ is a random noise component. Time series decomposition was performed on quarterly PWA concentrations and deposition rates, as well as subsets thereof by using the multiplicative decomposition model within Minitab Software (MINITAB, 2013). The multiplicative model consistently delivered better statistical measures than the additive model, implying that seasonal variations changed in magnitude with time. The linear trend in the dataset was obtained by using the deseasoned data:

$$(TxR)_{quarterly} = b_{quarterly} + m_{quarterly} \cdot \text{year} \quad (5)$$

where the intercept, $b_{quarterly}$, and slope, $m_{quarterly}$, are defined on a quarterly basis. Such trend estimates were determined for two time frames: one for the entire sampling period, i.e., 1989–2015, and a second for the latter 16 years, i.e., 1999–2015 (see below). Coefficients of determination (R^2) and p-values for both trendlines were determined and noted within graphs. Unless otherwise noted, a p-value of ≤ 0.05 was used as an indicator for a significant trend. Note that in the case of deposition rates, the slope of the trendline is expressed as a change in quarterly rate per year ($\text{kg ha}^{-1} \text{ qrt}^{-1} \text{ yr}^{-1}$) and the intercept is expressed in $\text{kg ha}^{-1} \text{ qrt}^{-1}$. Thus, to obtain estimates of the yearly deposition rate changes per year and calculate yearly deposition rates at any given time using the trendline equation, both the slope and the intercept need to be multiplied by 4 to account for the 4 quarters. In addition, the modeled quarterly values ($M_{quarter}$), or fitted values, were generated by multiplying the corresponding trend and seasonal components:

$$M_{quarter} = T_{quarter} \times S_{quarter} \quad (6)$$

$M_{quarter}$ are plotted in the time series graphs to visualize the seasonal patterns including their variations in amplitudes and shapes within and among species plots. Seasonality indices provide a measure of the season's variation from the average as given by the trend line and are

presented in the text when appropriate.

Comparisons between Paradise and Tahoma Woods data since 1999 were performed with paired student t-tests using p-values ≤ 0.05 to demonstrate significant differences (SPSS, 2017). Quarterly Tahoma Woods data were downloaded from the NADP website (NADP, 2019) and processed as indicated in the SI. Principal component analysis (PCA) is regularly used in environmental science to identify components that correlate with each other and assess their significance in the observed variance of the data (A. M. Johansen and Hoffmann, 2004; Orellana et al., 2019). In this way, PCA extracts a set of orthogonal components that are representative of different species sources. PCA was performed with Varimax Rotation (SPSS, 2017). Multiple linear regression analysis was used to model proton concentrations based on analyzed species (SPSS, 2017). For these latter analyses, non-sea-salt (NSS) fractions were computed by using Na^+ as the sea salt (SS) tracer and subtracting from a given component the SS contribution based on their relative abundances found in typical sea water (e.g., (Johansen et al., 1999)).

3. Results and discussion

3.1. Trend analysis of PWA quarterly concentrations and deposition rates

Quarterly average concentrations and deposition rates for SO_4^{2-} , NO_3^- and NH_4^+ are plotted in Fig. 1. Concentrations, in $\mu\text{eq L}^{-1}$, are shown in the left panel (A, C, and E), and respective deposition rates in $\text{kg S or N ha}^{-1} \text{ quarter}^{-1}$ and in $\text{meq m}^{-2} \text{ quarter}^{-1}$ are shown in the right panel (B, D, and F). Modeled data refers to Eqn. (6) including the entire sampling period (1989–2015) and provides a visual of the amplitude of seasonality and the difference between seasons. Trend line equations and corresponding R^2 and p-values for significance of the trend are noted within each graph, for time frames 1989–2015 (solid lines) and 1999–2015 (dashed lines). SO_4^{2-} and NO_3^- concentrations show significant negative trends, with the SO_4^{2-} trend of $0.177 \mu\text{eq L}^{-1} \text{ yr}^{-1}$ being a factor of 2.4 times that observed for NO_3^- , $0.074 \mu\text{eq L}^{-1} \text{ yr}^{-1}$. While NH_4^+ concentrations seem to be increasing with time, the p-value of 0.17 is deemed not significant. However, when considering data since 1999 only (which is when Tahoma Woods came online), the significance in trend increases ($p = 0.09$) and the

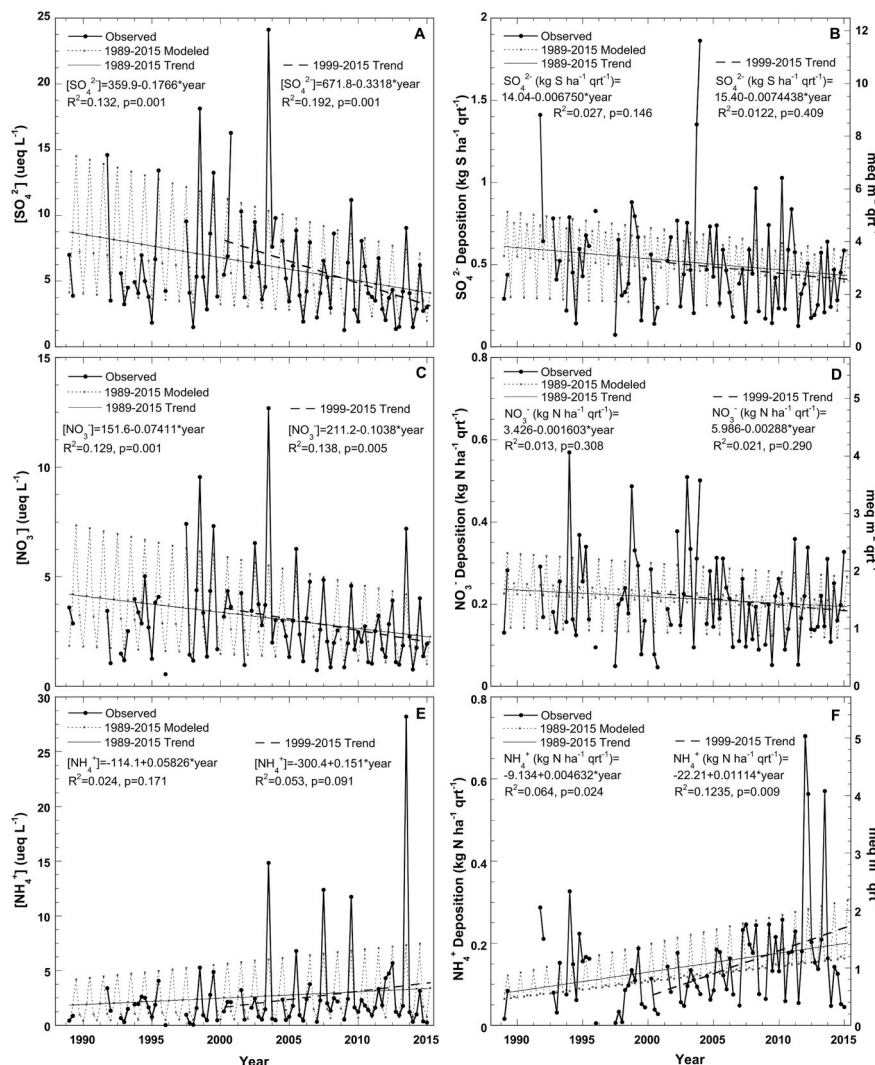


Fig. 1. Precipitation weighted quarterly average concentrations and respective quarterly deposition rates at Paradise, Mt. Rainier National Park between 1989 and 2015: sulfate (A, B), nitrate (C, D) and ammonium (E, F). Trendlines and equations are provided for 1989–2015 (solid lines) and 1999–2015 (dashed lines). Modeled data (dotted lines) are the output from the multiplicative decomposition model for 1989–2015 (see methods).

associated slope is larger by a factor of 2.6: 0.058 vs. $0.151 \mu\text{eq L}^{-1} \text{yr}^{-1}$ (see Fig. 1E). A similar significant trend of $0.13 \mu\text{eq L}^{-1} \text{yr}^{-1}$ is observed in the last 10 years (2006–2015) at Tahoma Woods (National Park Service, 2018). Seasonality indices for SO_4^{2-} , NO_3^- , and NH_4^+ show that concentrations are always largest in the summer quarter, with concentrations of 68%, 77% and 124% above the averages, respectively. Peaking NH_4^+ concentrations at Paradise during 4 summer seasons, 2003, 2007, 2009 and 2013 may be in part driving the positive trend. Summer seasons are typically characterized by higher concentrations due to lower precipitation volumes, however, the extreme peaks seen for NH_4^+ are more pronounced and correlate with peaks observed for SO_4^{2-} and NO_3^- (Fig. 1A and C), and K^+ (Fig. S5C). Coinciding higher than normal concentrations for these species were also observed at Tahoma Woods and Marblemount NADP sites, as well as in 2003 at the NADP site La Grande (not shown), and may stem from wild fires that occurred during the respective summers that engulfed large parts of the state. This observation is supported by the fact that K^+ and NH_4^+ are typical tracers for biomass burning. Decreasing concentrations for SO_4^{2-} and NO_3^- after around 2001 are likely attributed to effective efforts in emission reductions from a nearby power plant, located 80 km west of Mount Rainier National Park in Centralia, WA (Cummins, 2014).

In terms of deposition rates, while the overall trends for the three main species discussed so far remain the same as was observed for concentrations, the statistical significance of these trends change. For SO_4^{2-} and NO_3^- the negative trends in deposition rate are statistically less significant, with $p = 0.146$ and $p = 0.308$, respectively (Fig. 1B and D), while the positive NH_4^+ deposition trend is significant, with $p = 0.024$ (Fig. 1F). Note that deposition rates are plotted on a quarterly basis and thus the magnitude of the y-axis is smaller by an expected factor of 4 compared to yearly averages. Inspection of the deposition trends after 1999 show that the respective trends become more pronounced, in particular for NH_4^+ deposition, where the slope increased by a factor of 2.4 with a new $p = 0.009$ (see Fig. 1F). Seasonality indices for SO_4^{2-} , NO_3^- , and NH_4^+ deposition show that highest rates occur during spring quarter, with increased values compared to averages by 35%, 38%, and 52%, respectively. Modeled NH_4^+ deposition rates display a significantly different pattern from that observed in the other graphs in that the other quarters, i.e., winter, summer and fall seasons are characterized by similar seasonal contributions of 17% below averages (Fig. 1F).

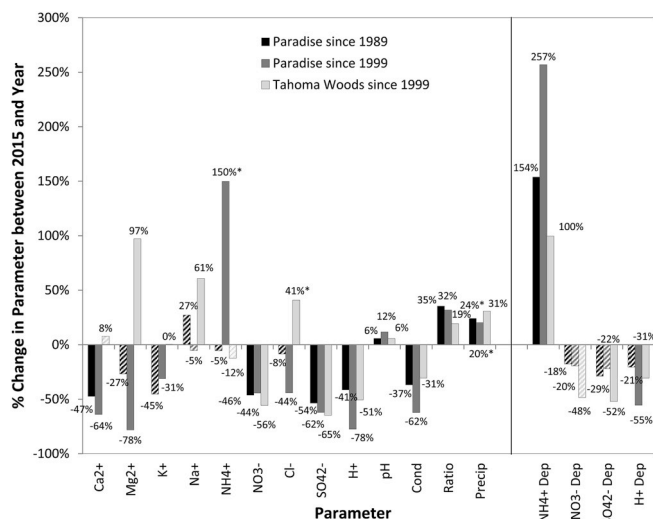


Fig. 2. %Change in magnitude of parameters in 2015, compared to 1989 or 1999, as indicated. Solid bars show significant differences as determined by the significant trend slopes in quarterly averages ($p \leq 0.05$, with exception for numbers with *, for which $p \leq 0.1$.) Four parameters to the right of the dividing line are for deposition rates.

For a visual comparison of trends at both Paradise and Tahoma Woods, the % change in each parameter between (i) 2015 and 1989, relative to 1989, and (ii) 2015 and 1999, relative to 1999, is plotted in Fig. 2. Statistically significant trends with $p \leq 0.05$ are shown in solid bars and trends with $p \leq 0.1$ are denoted with an asterisk. For instance, as seen in Fig. 1F, quarterly NH_4^+ deposition increased by $0.0046 \text{ kg N ha}^{-1} \text{ quarter}^{-1} \text{ yr}^{-1}$ since 1989, which translates into a 154% change between 1989 and 2015 and is plotted as a solid black column for NH_4^+ deposition to the right of the dividing line in Fig. 2. When looking at trends since 1999, NH_4^+ deposition increased significantly by 257% at Paradise and 100% at nearby Tahoma Woods. As found above, while concentrations of acidic species SO_4^{2-} and NO_3^- decrease significantly across the board, between 54% and 65%, respective deposition decreases significantly only for SO_4^{2-} at Tahoma Woods, by 52% between 1999 and 2015. These observations of NH_4^+ deposition increases, particularly in the past decade, as well as reductions in SO_4^{2-} and NO_3^- concentrations and depositions are consistent with those found elsewhere in the US (Butler et al., 2016; Clow et al., 2015; Fakhraei et al., 2016; Lehmann et al., 2005; Zhang et al., 2018).

Another parameter of ecological significance and frequently studied in association with SO_4^{2-} , NO_3^- and NH_4^+ is the concentration and deposition of protons (H^+), shown in Fig. 3A and B, respectively. While H^+ concentrations decreased significantly over the 26-year study by $0.087 \mu\text{eq L}^{-1} \text{yr}^{-1}$ (41% reduction, Fig. 2), the concentration graph (Fig. 3A) shows that levels peaked around 2001, which coincides with elevated SO_4^{2-} and NO_3^- and may stem from the regional pollution from the nearby power plant in Centralia. Correspondingly, pH values increased by 6% and to 5.6 in 2015 (Fig. 3C). A pH 5.6 is that of water in equilibrium with current atmospheric $\text{CO}_2(\text{g})$ concentrations, indicating that in recent years acid precipitation and deposition at Paradise seem to have ceased. This is likely in part a consequence of increased emissions of acid neutralizing species, including NH_4^+ . A similar pattern is observed at Tahoma Woods, where the pH increased by 6% to 5.4 from 1999 to 2015. Associated H^+ deposition rates decreased significantly at both Paradise and Tahoma Woods since 1999, by 55% and 31%, respectively.

Additional significant trends observed at both Paradise and Tahoma Woods for all investigated time frames are precipitation, conductivity and the ratio between positive and negative ions. Precipitation increased since 1999, by 20% and 31%, at Paradise (Fig. 3D) and Tahoma Woods, respectively. At Paradise, it seems that the concurrent increase in precipitation and decrease in SO_4^{2-} and NO_3^- concentrations is the cause for why respective deposition rates did not change significantly. The reduction in conductivity (Fig. S5A) is likely a manifestation of lower concentrations of anions and protons that are associated with pollutant sources. The significant increasing trend in the ratio of positive vs. negative charges (Fig. S5B) is a consequence of the same observation with the additional argument that anions decreased more rapidly than the cations. The fact that the positive over negative ion ratio tends to be larger than 1 is due to the fact that bicarbonate species and organic acids are not determined in this study and they are thus missing from the denominator.

3.2. Comparison between paradise and Tahoma Woods observations

Paired student t-tests were performed on all quarterly species concentrations and deposition rates between Paradise and Tahoma Woods from fall of 1999 to spring of 2015. Concentration and deposition averages, and p-values are listed in Table 1. P-values of ≤ 0.05 , indicating significant differences between the two sites at the 95% confidence interval, were found for NO_3^- , Cl^- , H^+ , Ca^{2+} , conductivity, precipitation and deposition rates for all discussed species. Notable is that precipitation amounts were higher at Paradise by a factor of 2.1 and that deposition rates were also higher at Paradise by 31%–75% for H^+ and NH_4^+ , respectively. Quarterly deposition rates were tested for differences by season (Table S1). In general, significantly higher

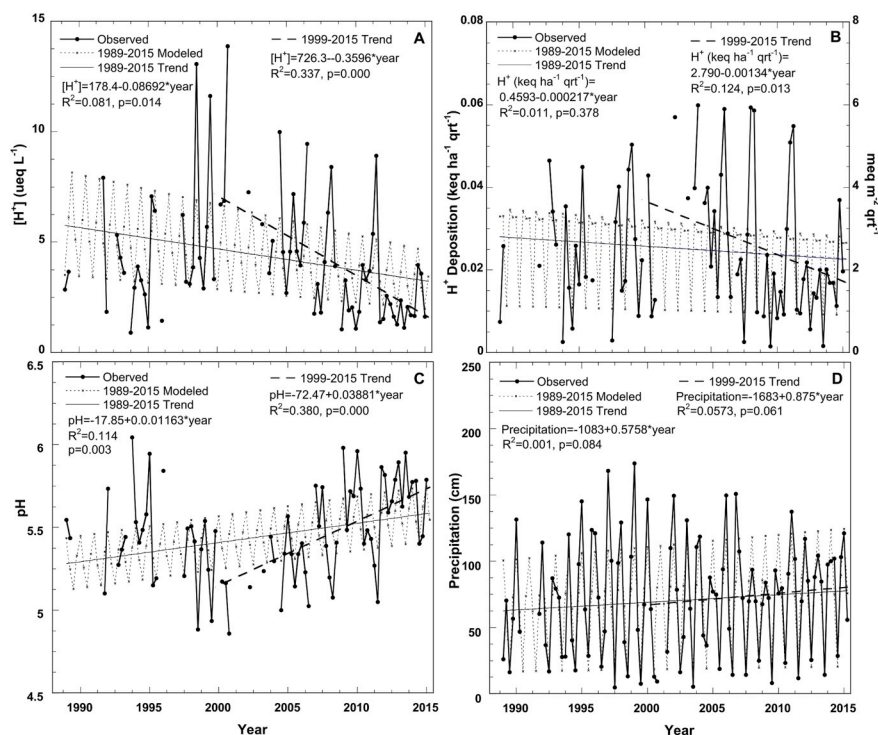


Fig. 3. Precipitation weighted quarterly average concentration for protons (A), respective quarterly deposition rates (B), pH (C), and precipitation (D) at Paradise, Mt. Rainier National Park between 1989 and 2015. Trendlines and equations are provided for 1989–2015 (solid lines) and 199–2015 (dashed lines). Modeled data (dotted lines) are the output from the multiplicative de-composition model for 1989–2015 (see methods).

Table 1
Comparison of Paradise and Tahoma Woods Quarterly Precipitation and Deposition Averages since 1999 (n = 41, unless otherwise noted).

Component	Averages and Standard Deviations (ueq L ⁻¹ unless otherwise noted)				p*
	Paradise	SD	Tahoma Woods	SD	
SO ₄ ²⁻	5.42	4.19	4.78	2.63	0.170
NO ₃ ⁻	2.62	2.04	3.92	3.13	0.000
NH ₄ ⁺	2.11	2.80	2.36	2.13	0.396
H ⁺ (n = 36)	4.07	2.89	5.83	1.83	0.001
Cl ⁻ (n = 35)	6.38	3.99	9.00	3.65	0.002
Na ⁺	5.83	4.08	6.89	3.14	0.138
K ⁺	1.05	2.91	0.54	0.90	0.260
Mg ²⁺	2.20	2.51	1.53	0.68	0.108
Ca ²⁺	2.26	1.62	1.52	0.73	0.002
Cond. (uS cm ⁻¹ , Nn = 36)	3.34	1.67	4.54	1.06	0.000
Precip. (cm, Nn = 62)	73.5	40.8	34.6	18.0	0.000
SO ₄ ²⁻ Dep. (kg S (ha qrt) ⁻¹)	0.51	0.33	0.27	0.24	0.000
NO ₃ ⁻ Dep. (kg S (ha qrt) ⁻¹)	0.21	0.11	0.15	0.07	0.002
NH ₄ ⁺ Dep. (kg S (ha qrt) ⁻¹)	0.14	0.09	0.08	0.06	0.000
H ⁺ Dep. ((keq (ha qrt) ⁻¹), n = 36)	0.027	0.017	0.021	0.007	0.028

*p ≤ 0.05, in bold, denotes significant difference at 95% confidence for paired t-test.

concentrations were observed at Paradise during the winter months, which is the season with largest precipitation amounts.

3.3. Five-year averaged deposition rates

Precipitation weighted average quarterly deposition rates for SO₄²⁻, NO₃⁻, NH₄⁺ and H⁺ were calculated over the following 5-year time spans: 1989–1994 (6 years), 1995–1999, 2000–2005, 2006–2010, and 2011–2015. Resulting estimates of quarterly rates for each of the 5-year periods are shown in stacked bars (Fig. 4A–C) to visualize measures of yearly deposition rates. Tahoma Woods data (in narrow bars) was included for comparison for the existing 3 timeframes: 1999–2005, 2006–2010, and 2011–2015. Consistent with previous observations in trends (section 3.1), deposition rates generally peak in 2001–2005 and then decrease. Furthermore, as Student t-tests revealed (section 3.2),

deposition rates at Paradise exceed or are similar to those observed at Tahoma Woods despite the fact that precipitation concentrations are generally higher at Tahoma Woods. This is a consequence of the significantly higher precipitation volumes at Paradise; an observation not uncommon for high-elevation areas, which further supports the need for long-term sampling at such sensitive locations (Fakhraei et al., 2016; Sullivan et al., 2018). An exception to the general decrease in deposition rates is the N deposition that stems from NH₄⁺ (Fig. 4B, hatched stacked bars), which at Paradise, has increased significantly in the last 5 years. A general upward trend in background concentrations is attributed to agricultural activities and has been seen elsewhere (Butler et al., 2016; Du et al., 2014; Lehmann et al., 2005; Zhang et al., 2018). In the Great Smoky Mountains, a recent study found that NH₄⁺ significantly contributed to N deposition suggesting that focus needs to be directed toward controlling NH₃ emissions (Fakhraei et al., 2016). At

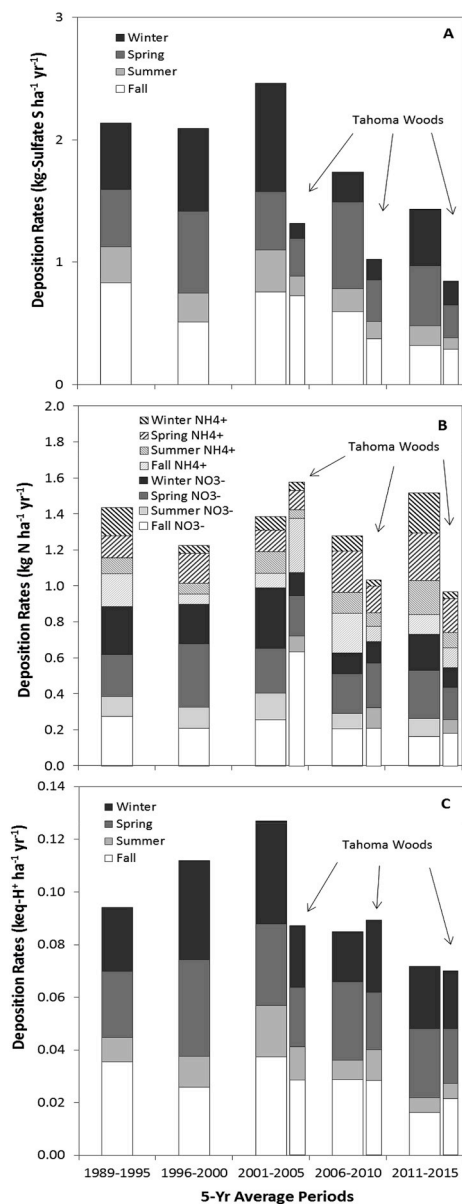


Fig. 4. Stacked precipitation weighted quarterly 5-year average deposition rates providing estimated yearly deposition rates for sulfur from SO_4^{2-} (A), nitrogen from NO_3^- and NH_4^+ (B), and H^+ (C). Data for Paradise (1989, 2015) are shown in wide and for Tahoma Woods (1999–2015) in narrow columns, as indicated.

Paradise, this trend is exacerbated by episodic peaks from wildfires. Overall, N deposition values at Paradise are consistent with those observed at other high elevation sites in Western North America including the US and Canadian Rocky Mountains (Clow et al., 2015; Lafreniere and Sinclair, 2011; Wasiuta et al., 2015). Deposition of N in the form of NH_4^+ may also lead to further acidification of the environment as nitrification to NO_2^- and further to NO_3^- is associated with the formation of 2 additional H^+ (Fakhraei et al., 2016). Thus, although direct acid deposition has decreased, the continued acidification of soils through NH_4^+ deposition and oxidation augments the effect from past acid precipitation thus further hampering recovery of delicate soil chemistry in these areas (Sullivan et al., 2018).

3.4. Chemical associations and sources

To obtain an overview of potential correlations between

Table 2

Rotated Principal Component Matrix of species concentrations, respective NSS contributions and precipitation for individual samples ($\mu\text{eq L}^{-1}$ unless otherwise noted).

Principal Component (% of Variance)/Parameter	PC1	PC2	PC3	PC4	PC5
	40.5	16.6	12.5	9.2	8.2
H^+	0.832	-0.126	0.142	-0.117	0.301
Conductivity ($\mu\text{S cm}^{-1}$)	0.718	0.450	0.378	0.025	0.213
Cl^-	0.113	0.017	0.898	0.091	0.346
NSS- Cl^-	0.038	0.025	0.028	0.042	0.969
NO_3^-	0.783	0.078	-0.058	0.362	-0.027
SO_4^{2-}	0.858	0.226	0.264	0.232	-0.029
NSS- SO_4^{2-}	0.876	0.234	0.156	0.231	0.003
Na^+	0.097	0.002	0.950	0.071	-0.266
NH_4^+	0.202	0.925	-0.029	0.007	-0.063
K^+	0.098	0.972	0.104	0.026	-0.017
NSS- K^+	0.095	0.975	0.070	0.023	-0.007
Mg^{2+}	0.153	0.475	0.738	0.299	0.097
NSS- Mg^{2+}	0.125	0.654	0.177	0.350	0.369
Ca^{2+}	0.277	0.062	0.194	0.916	0.024
NSS- Ca^{2+}	0.274	0.063	0.108	0.929	0.049
NOAA Precip.(cm)	-0.519	-0.093	0.093	-0.213	0.122

Extraction Method: Principal Component Analysis, varimax rotation, $n = 572$, rotation converged in 6 iterations.

components and sources, PCA was performed on individual evaporation corrected samples ($N = 572$). Included in the analysis were precipitation amount, and concentrations of all species including non-sea-salt (NSS) fractions of the following: SO_4^{2-} , Cl^- , K^+ , Mg^{2+} , and Ca^{2+} . Five principal components (PC) with eigenvalues > 1 were extracted. The Varimax rotated component loadings and their respective % of variances are shown in Table 2. Component loadings larger than 0.5 and smaller than -0.5 are in bold and considered to be significant in their association with the component. PC1 accounts for 40.5% of the variance and is characteristic of acidity in its association with H^+ , NO_3^- and NSS- SO_4^{2-} , also adding significantly to overall conductivity. The correlation between NO_3^- and NSS- SO_4^{2-} suggests common precursors, i.e., SO_2 and NO_x emitted from anthropogenic sources such as fossil fuel burning. The observed anti-correlation with precipitation indicates that higher volumes of precipitation lead to the dilution of these particular chemical components. PC2 (variance of 16.6%) is representative of biomass burning (BB), as it is described by the typical tracers NH_4^+ and K^+ , with some NSS- Mg^{2+} , species that contribute to neutralization of acidity and therefore show a slight negative relationship with H^+ . PC3 (12.5% variance) seems to be characteristic of SS (Na^+ , Cl^- , Mg^{2+}). PC4 and PC5 are similar in % of variance, 9.2 and 8.2, respectively, with PC4 potentially representing a soil component (NSS- Ca^{2+}) and PC5 a somewhat acidic NSS- Cl^- component (loading for H^+ is 0.301). Exclusion of the NSS fractions in the PCA results in 3 PCs that correspond to the first 3 PCs obtained above; however, PC2 and PC3 are swapped in order and closer to each other in %variance (17 and 16%) (Table S2 in SI). Thus, PC1, describing acidity remained predominant. Analogous results were obtained from PCA performed on volume-weighted quarterly averages ($N = 73$, Table S3). To investigate differences in seasons, PCA was also performed on each subset of quarterly averages (Tables S4 and S5). In general, the same PCs emanated with a few changed orders and splits between different components. To briefly summarize: in winter ($N = 20$), the acidic component, PC1 (H^+), was associated with Cl^- and Mg^{2+} , rather than the typical NO_3^- and SO_4^{2-} , which appeared instead in PC2 associated with K^+ and Ca^{2+} , indicating potential soil sources; in spring ($N = 18$), PC1 was typical of SS, including SO_4^{2-} , indicating that the characteristic strong spring winds effectively blew SS aerosols toward the mountains, and H^+ appeared in PC3 with NO_3^- ; in summer ($N = 17$), acidity appeared again in PC1, strongly associated with SO_4^{2-} , NO_3^- , and conductivity, while PC2 contributed significantly to neutralizing H^+ with the typical BB

Table 3
Coefficients for multivariate linear regression analysis with H^+ (μM) as Dependent variable.

Independent Variables	Unstandardized Coefficients		Standardized Coefficients	t	Sig.	95.0% Confidence Interval for B	
	B	Std. Error	Beta			Lower Bound	Upper Bound
(Constant)	2.20	0.19		11.36	0.000	1.82	2.58
[NSS-SO ₄ ²⁻] (μM)	0.85	0.06	0.742	14.07	0.000	0.73	0.96
[NSS-Cl ⁻] (μM)	0.29	0.03	0.320	10.06	0.000	0.24	0.35
[NSS-Mg ²⁺] (μM)	-0.89	0.23	-0.177	-3.82	0.000	-1.34	-0.43
[NSS-K ⁺] (μM)	-0.21	0.05	-0.186	-4.69	0.000	-0.30	-0.12
[NSS-Ca ²⁺] (μM)	-0.54	0.11	-0.194	-5.14	0.000	-0.75	-0.33
[NO ₃ ⁻] (μM)	0.17	0.06	0.154	3.11	0.002	0.06	0.28

signatures of NH_4^+ and K^+ ; and in fall ($N = 18$), acidity in PC1 was associated with the regular SO_4^{2-} , NO_3^- , and conductivity, but also with NH_4^+ , while PC2 was characteristic of SS, and Ca^{2+} appeared with NO_3^- in PC3.

In the context of sources and sinks of H^+ , these results show that depending on season, a significant portion of SO_4^{2-} is SS derived while NO_3^- may have a soil component, neither of which contribute to acidity. NH_4^+ and K^+ seem strongly associated with sporadic summer wild fires, that are known to emit NH_3 (g), KOH (s) and K_2CO_3 (s) and are acid neutralizing. $NSS-Ca^{2+}$ and $NSS-Mg^{2+}$ are in the alkaline earth group and provide alkalinity in the form of their (hydr)oxides and carbonates. In an attempt to perform a mass balance of H^+ it is thus important to use the NSS fractions of SO_4^{2-} and alkali and alkaline earth cations. The aforementioned potentially soil-derived NO_3^- component could stem from the re-suspension of soils and, depending on its provenance, not contribute to the net flux of N deposition to soils. Assuming that all Na^+ is SS derived, on average, the SS contributions to total SO_4^{2-} , K^+ , and Ca^{2+} were found to be between 9 and 10%, while for Mg^{2+} and Cl^- , they were considerably higher, averaging 50 and 83%, respectively.

3.5. Proton sources and sinks

With information obtained in the PCA, acidity seems to be positively associated with $NSS-SO_4^{2-}$ and NO_3^- and negatively associated with $NSS-K^+$ and NH_4^+ (BB) as well as with $NSS-Mg^{2+}$ and $NSS-Ca^{2+}$ (soil-derived). In addition, some acidity seems to be related to $NSS-Cl^-$ (in PC5, Table 2). To determine the relative contributions of each of these species to H^+ , multivariate linear regression analysis was performed using all individual samples ($N = 572$). With H^+ as the dependent variable, and total and NSS concentrations of all parameters as independent variables, a stepwise forward process eliminated those independent parameters that were not significant in describing H^+ ($p \geq 0.05$). The best model, with an R^2 of 0.507, included the NSS fractions of SO_4^{2-} , Cl^- , Mg^{2+} , K^+ , and Ca^{2+} , and NO_3^- , and excluded NH_4^+ . The model output, including coefficients and significance levels, are shown in Table 3 (ANOVA and model summaries are in Table S6). The order of independent parameters in the table follows the order in which the forward stepwise method identified the significance of each parameter in modeling the dependent variable: from $NSS-SO_4^{2-}$ being the most significant to NO_3^- being the least significant. Standardized coefficients (Beta) are computed so that the variances of dependent and independent variables are 1, therefore, they provide a normalized measure of how many standard deviations a dependent variable will change, per standard deviation change in the predictor variable. Thus, $NSS-SO_4^{2-}$ has the largest effect on H^+ , followed by $NSS-Cl^-$. All three acid-neutralizing species have expectedly negative effects that are also significantly smaller. NO_3^- has the least effect on acidity overall and it is positive. The unstandardized coefficients provide a direct measure of how many moles of H^+ are supplied by each mole of the independent component, and they form the coefficients in the following linear

regression equation (all concentrations in μM):

$$[H^+] = 0.85 [NSS-SO_4^{2-}] + 0.29 [NSS-Cl^-] + 0.17 [NO_3^-] - 0.89 [NSS-Mg^{2+}] - 0.54 [NSS-Ca^{2+}] - 0.21 [NSS-K^+] + 2.2 \quad (7)$$

By way of an example, each mole of $NSS-SO_4^{2-}$ contributes 0.85 ± 0.06 mol of H^+ . Analogously, only 0.17 ± 0.06 mol of H^+ are provided by each mole of NO_3^- , which indicates that 83% of NO_3^- stems from sources other than those leading to H^+ formation. Of total $NSS-Cl^-$, 29% seem to contribute H^+ . Although the standardized coefficient for $NSS-Mg^{2+}$ indicates that it does not contribute much to neutralizing H^+ overall due to its relatively small concentration, 89% of the $NSS-Mg^{2+}$ that is present does lead to the neutralizing H^+ . By comparison, $NSS-Ca^{2+}$ and $NSS-K^+$, each contribute 54 and 21% of their molar concentrations in H^+ , respectively. When replacing the independent variable K^+ with its correlating BB component NH_4^+ , the model output is still $R^2 = 0.502$, however, the unstandardized coefficient for NH_4^+ is -0.06 , indicating that only 6% of NH_4^+ contributed to neutralizing H^+ (not shown). When forcing the inclusion of both K^+ and NH_4^+ , the latter results as insignificant ($p = 0.88$). These results confirm that K^+ is a larger contributor to acid neutralization than NH_4^+ , most likely from BB emissions and that acid neutralizing NH_3 from other sources is small by comparison. In relation to the PCA analysis, the acidifying factors $NSS-SO_4^{2-}$ and NO_3^- appear in PC1, while $NSS-Cl^-$ is represented in PC5, whereas the acid-neutralizing species are represented in PC2 ($NSS-K^+$ and $NSS-Mg^{2+}$) and PC 4 ($NSS-Ca^{2+}$).

The constant, 2.2 μM , is representative of a background level of H^+ , which represents a pH of 5.7. This value is very close to the pH of 5.6 which is that of pure water in equilibrium with CO_2 . Such a good match for a constant provides another indicator that the model is an adequate representation of H^+ sources and sinks.

4. Conclusions

Twenty-six years of field observations from a uniquely situated high-elevation site at Mount Rainier National Park reveal that SO_4^{2-} and NO_3^- concentrations in precipitation decreased between 1989 and 2015, while peaking in 2000–2001. Associated effective reduction in acid precipitation was most notably driven by decreases in SO_4^{2-} and thus S emissions. In the latter 15 years, however, NH_4^+ concentrations increased significantly, resulting in deposition rates rising from 0.27 to 0.96 $kg N ha^{-1} yr^{-1}$, the latter exceeding the 2015 deposition of N by NO_3^- of 0.74 $kg N ha^{-1} yr^{-1}$. Combined 2015 N deposition rates of 1.7 $kg N ha^{-1} yr^{-1}$ are below the lowest estimated CL of 2.0 $kg N ha^{-1} yr^{-1}$ (Clark et al., 2018; J J Williams et al., 2017), however, if current trends persist it can be extrapolated that this CL may be exceeded within the next 9–10 years.

These general observations are consistent with what has been seen in other parts of the US and Europe. Persistent emissions from agricultural activities and episodic releases from wild fires are contributing to enhanced NH_4^+ deposition, with detrimental effects on ecosystems through continuous fertilization and indirect acidification. The time

frame for repairing existing damage given these compounding effects is nebulous and specific to this particular environment. Therefore, knowledge of long-term deposition rate magnitudes and trends is of utmost importance to estimate the overall effect of pollutant deposition, in particular in delicate high-elevation areas such as at Mount Rainier. These results help to assess the effectiveness of current policies and shape future legislation to protect the most vulnerable ecosystems.

Declaration of interests

The authors declare that they have no known competing financial interests or personal relationships that could have appeared to influence the work reported in this paper.

Acknowledgments

Funding for this work was provided by the National Park Service Cooperative Agreement H9453070012. Numerous individuals assisted with field and laboratory work and their help is greatly appreciated. Special thanks are extended to all the Park Service Technicians that over the years were responsible for bucket placement, retrieval and shipment, Ben Wright for providing the windroses (in SI), and Lisa Stowe, CWU Chemistry Department Secretary, for facilitating bucket receipt and transfer at CWU.

Appendix A. Supplementary data

Supplementary data to this article can be found online at <https://doi.org/10.1016/j.atmosenv.2019.05.021>.

References

- Amann, M., Klimont, Z., Wagner, F., 2013. Regional and global emissions of air pollutants: recent trends and future scenarios. *Annu. Rev. Environ. Resour.* 38 (38), 31–55. <https://doi.org/10.1146/annurev-environ-052912-173303>.
- Baron, J.S., 2006. Hindcasting nitrogen deposition to determine an ecological critical load. *Ecol. Appl.* 16 (2), 433–439. [https://doi.org/10.1890/1051-0761\(2006\)016\[0433:hndtda\]2.0.co;2](https://doi.org/10.1890/1051-0761(2006)016[0433:hndtda]2.0.co;2).
- Benedict, K.B., Carrico, C.M., Kreidenweis, S.M., Schichtel, B., Malm, W.C., Collett, J.L., 2013. A seasonal nitrogen deposition budget for Rocky Mountain National Park. *Ecol. Appl.* 23 (5), 1156–1169. <https://doi.org/10.1890/12-1624.1>.
- Brockwell, P.J., Davis, R.A., 2016. Introduction to Time Series and Forecasting, third ed. Springer International Publishing Ag, Cham, pp. 1–425. <https://doi.org/10.1007/978-3-319-29854-2>.
- Butler, T., Vermeylen, F., Lehmann, C.M., Likens, G.E., Puchalski, M., 2016. Increasing ammonia concentration trends in large regions of the USA derived from the NADP/AMON network. *Atmos. Environ.* 146, 132–140. <https://doi.org/10.1016/j.atmosenv.2016.06.033>.
- Clark, C.M., Phelan, J., Doraiswamy, P., Buckley, J., Cajka, J.C., Dennis, R.L., Lynch, J., Nolte, C.G., Spero, T.L., 2018. Atmospheric deposition and exceedances of critical loads from 1800–2025 for the conterminous United States. *Ecol. Appl.* 28 (4), 978–1002. <https://doi.org/10.1002/eap.1703>.
- Clow, D.W., Roop, H.A., Nanus, L., Fenn, M.E., Sextstone, G.A., 2015. Spatial patterns of atmospheric deposition of nitrogen and sulfur using ion-exchange resin collectors in Rocky Mountain National Park, USA. *Atmos. Environ.* 101, 149–157. <https://doi.org/10.1016/j.atmosenv.2014.11.027>.
- Cummings, T., 2014. Air Quality Overview: Mount Rainier National Park, Rep. National Park Service, Fort Collins, CO NPS/PWRO/NRR—2014/848.
- Du, E.Z., de Vries, W., Galloway, J.N., Hu, X.Y., Fang, J.Y., 2014. Changes in wet nitrogen deposition in the United States between 1985 and 2012. *Environ. Res. Lett.* 9 (9). <https://doi.org/10.1088/1748-9326/9/9/095004>.
- Ellis, R.A., Jacob, D.J., Sulprizio, M.P., Zhang, L., Holmes, C.D., Schichtel, B.A., Blett, T., Porter, E., Pardo, L.H., Lynch, J.A., 2013. Present and future nitrogen deposition to national parks in the United States: critical load exceedances. *Atmos. Chem. Phys.* 13 (17), 9083–9095. <https://doi.org/10.5194/acp-13-9083-2013>.
- Fakhraei, H., Driscoll, C.T., Renfro, J.R., Kulp, M.A., Blett, T.F., Brewer, P.F., Schwartz, J.S., 2016. Critical loads and exceedances for nitrogen and sulfur atmospheric deposition in Great Smoky Mountains National Park, United States. *Ecosphere* 7 (10). <https://doi.org/10.1002/ecs2.1466>.
- Fenn, M.E., Bytnerowicz, A., Liptzin, D., 2013. Nationwide maps of atmospheric deposition are highly skewed when based solely on wet deposition. *Bioscience* 62 (7). <https://doi.org/10.1525/bio.2012.62.7.18>.
- Fenn, M.E., et al., 2003. Nitrogen emissions, deposition, and monitoring in the western United States. *Bioscience* 53 (4), 391–403. [https://doi.org/10.1641/0006-3568\(2003\)053\[0391:medami\]2.0.co;2](https://doi.org/10.1641/0006-3568(2003)053[0391:medami]2.0.co;2).
- Fenn, M.E., Ross, C.S., Schilling, S.L., Baccus, W.D., Larrabee, M.A., Lofgren, R.A., 2012. Atmospheric deposition of nitrogen and sulfur and preferential canopy consumption of nitrate in forests of the Pacific Northwest, USA. *For. Ecol. Manag.* 302, 240–253. <https://doi.org/10.1016/j.foreco.2013.03.042>.
- Fowler, D., et al., 2013. The global nitrogen cycle in the twenty-first century. *Phil. Trans. Biol. Sci.* 368 (1621). <https://doi.org/10.1098/rstb.2013.0164>.
- Geiser, L.H., Jovan, S.E., Glavich, D.A., Porter, M.K., 2011. Lichen-based critical loads for atmospheric nitrogen deposition in Western Oregon and Washington Forests, USA. *Environ. Pollut.* 158 (7), 2412–2421. <https://doi.org/10.1016/j.envpol.2010.04.001>.
- Ghaly, A.E., Ramakrishnan, V.V., 2015. Nitrogen sources and cycling in the ecosystem and its role in air, water and soil pollution: a critical review. *Journal of Pollution Effects and Control* 3 (2), 136. <https://doi.org/10.4172/2375-4397.1000136>.
- Glavich, D.A., Geiser, L.H., 2008. Potential approaches to developing lichen-based critical loads and levels for nitrogen, sulfur and metal-containing atmospheric pollutants in North America. *Bryologist* 111 (4), 638–649. <https://doi.org/10.1639/0007-2745-111.4.638>.
- Greaver, T.L., et al., 2012. Ecological effects of nitrogen and sulfur air pollution in the US: what do we know? *Front. Ecol. Environ.* 10 (7), 365–372. <https://doi.org/10.1890/110049>.
- Gu, D., Wang, Y., Smeltzer, C., Liu, Z., 2013. Reduction in NOx emission trends over China: regional and seasonal variations. *Environ. Sci. Technol.* 47 (22), 12912–12919. <https://doi.org/10.1021/es401727e>.
- Hundey, E.J., Russell, S.D., Longstaffe, F.J., Moser, K.A., 2016. Agriculture causes nitrate fertilization of remote alpine lakes. *Nat. Commun.* 7. <https://doi.org/10.1038/ncomms10571>.
- Johansen, A.M., Hoffmann, M.R., 2004. Chemical characterization of ambient aerosol collected during the northeast monsoon season over the Arabian Sea: anions and cations. *Journal of Geophysical Research-Atmospheres* 109 (D5).
- Johansen, A.M., Siefert, R.L., Hoffmann, M.R., 1999. Chemical characterization of ambient aerosol collected during the southwest-monsoon and inter-monsoon seasons over the Arabian Sea: anions and cations. *J. Geophys. Res.* 104, 26325–26347.
- Kaushal, S.S., Likens, G.E., Utz, R.M., Pace, M.L., Grese, M., Yepsen, M., 2013. Increased river alkalization in the eastern U.S. *Environ. Sci. Technol.* 47 (18), 10302–10311. <https://doi.org/10.1021/es401046s>.
- Klimont, Z., Smith, S.J., Cofala, J., 2013. The last decade of global anthropogenic sulfur dioxide: 2000–2011 emissions. *Environ. Res. Lett.* 8 (1). <https://doi.org/10.1088/1748-9326/8/1/014003>.
- Lafreniere, M.J., Sinclair, K.E., 2011. Snowpack and precipitation chemistry at a high altitude site in the Canadian Rocky Mountains. *J. Hydrol.* 409 (3–4), 737–748. <https://doi.org/10.1016/j.jhydrol.2011.09.007>.
- Lajtha, K., Jones, J., 2013. Trends in cation, nitrogen, sulfate and hydrogen ion concentrations in precipitation in the United States and Europe from 1978 to 2010: a new look at an old problem. *Biogeochemistry* 116 (1–3), 303–334. <https://doi.org/10.1007/s10533-013-9860-2>.
- Lehmann, C.M.B., Bowersox, V.C., Larson, S.M., 2005. Spatial and temporal trends of precipitation chemistry in the United States, 1985–2002. *Environ. Pollut.* 135 (3), 347–361. <https://doi.org/10.1016/j.envpol.2004.11.016>.
- Liu, B., Kang, S.C., Sun, J.M., Zhang, Y.L., Xu, R., Wang, Y.J., Liu, Y.W., Cong, Z.Y., 2013. Wet precipitation chemistry at a high-altitude site (3,326 m a.s.l.) in the southeastern Tibetan Plateau. *Environ. Sci. Pollut. Control Ser.* 20 (7), 5013–5027. <https://doi.org/10.1007/s11356-012-1379-x>.
- Lynch, J.A., Bowersox, V.C., Grimm, J.W., 2000. Acid rain reduced in Eastern United States. *Environ. Sci. Technol.* 34 (6), 940–949. <https://doi.org/10.1021/es9901258>.
- MINITAB, 2013. Minitab for Windows, vol. 16 Minitab Inc., State College, PA.
- Muri, G., 2013. Atmospheric deposition chemistry in a subalpine area of the Julian Alps, North-West Slovenia. *J. Limnol.* 72 (2), 291–300. <https://doi.org/10.4081/jlimnol.2013.e23>.
- Murray, G.L.D., Kimball, K.D., Hill, L.B., Hislop, J.E., Weathers, K.C., 2013. Long-term trends in cloud and rain chemistry on mount Washington, New Hampshire. *Water Air Soil Pollut.* 224 (9). <https://doi.org/10.1007/s11270-013-1653-7>.
- NADP, 2009. NADP QAAG Special Study 2009-04, QAAG Special Study: Criterion 4. NADP Program Office, Champlain, Illinois. <http://nadp.slh.wisc.edu/lib/misc/Criterion4report.pdf>.
- NADP, 2019. NADP Program Office. Wisconsin State Laboratory of Hygiene, 465 Henry Mall, Madison, WI 53706. <https://nadp.slh.wisc.edu/data/sites/siteDetails.aspx?net=NTN&id=WA99>.
- Naftz, D.L., Schuster, P.F., Johnson, C.A., 2011. A 50-year record of NOx and SO2 sources in precipitation in the Northern Rocky Mountains, USA. *Geochem. Trans.* 12. <https://doi.org/10.1186/1467-4866-12-4>.
- Nanus, L., Clow, D.W., Saros, J.E., Stephens, V.C., Campbell, D.H., 2012. Mapping critical loads of nitrogen deposition for aquatic ecosystems in the Rocky Mountains, USA. *Environ. Pollut.* 166, 125–135. <https://doi.org/10.1016/j.envpol.2012.03.019>.
- National Park Service, N., 2006. NPS Organic Act. pp. 1916. <http://www.nps.gov/protect/> (N. P. S. M. Policies).
- National Park Service, N., 2018. National Park Conditions and Trends. <https://www.nps.gov/subjects/air/park-conditions-trends.htm>.
- Orellana, S., Johansen, A.M., Gazis, C., 2019. Geographic classification of U.S. Washington State wines using elemental and water isotope composition. *Food Chem.* X 1, 100007. <https://doi.org/10.1016/j.fochx.2019.100007>.
- Pardo, L.H., et al., 2010. Effects of nitrogen deposition and empirical nitrogen critical loads for ecoregions of the United States. *Ecol. Appl.* 21 (8), 3049–3082.
- Pardo, L.H., et al., 2011. Effects of nitrogen deposition and empirical nitrogen critical loads for ecoregions of the United States. *Ecol. Appl.* 21 (8), 3049–3082.
- Prema, V., Rao, K.U., 2015. Time series decomposition model for accurate wind speed forecast. *Renewables. Wind, Water, and Solar* 2 (1), 18. <https://doi.org/10.1186/s40807-015-0018-9>.
- Sheibley, R.W., Enache, M., Swarzenski, P.W., Moran, P.W., Foreman, J.R., 2014.

- Nitrogen deposition effects on diatom communities in lakes from three national parks in Washington state. *Water Air Soil Pollut.* 225 (2). <https://doi.org/10.1007/s11270-013-1857-x>.
- Smith, S.J., van Aardenne, J., Klimont, Z., Andres, R.J., Volke, A., Arias, S.D., 2011. Anthropogenic sulfur dioxide emissions: 1850-2005. *Atmos. Chem. Phys.* 11 (3), 1101–1116. <https://doi.org/10.5194/acp-11-1101-2011>.
- SPSS, I., 2017. *SPSS Statistics*. SPSS Inc., Chicago.
- Sullivan, T.J., et al., 2018. Air pollution success stories in the United States: the value of long-term observations. *Environ. Sci. Policy* 84, 69–73. <https://doi.org/10.1016/j.envsci.2018.02.016>.
- Vet, R., et al., 2014. A global assessment of precipitation chemistry and deposition of sulfur, nitrogen, sea salt, base cations, organic acids, acidity and pH, and phosphorus. *Atmos. Environ.* 93 (0), 3–100. <https://doi.org/10.1016/j.atmosenv.2013.10.060>.
- Wasiuta, V., Lafreniere, M.J., Norman, A.-L., 2015. Atmospheric deposition of sulfur and inorganic nitrogen in the Southern Canadian Rocky Mountains from seasonal snow-packs and bulk summer precipitation. *J. Hydrol.* 523, 563–573. <https://doi.org/10.1016/j.jhydrol.2015.01.073>.
- Williams, J.J., Lynch, J.A., Saros, J.E., Labou, S.G., 2017. Critical loads of atmospheric N deposition for phytoplankton nutrient limitation shifts in western U.S. mountain lakes. *Ecosphere* 8 (10), e01955. <https://doi.org/10.1002/ecs2.1955>.
- Williams, M.W., Tonnessen, K.A., 2000. Critical loads for inorganic nitrogen deposition in the Colorado Front Range, USA. *Ecol. Appl.* 10 (6), 1648–1665. <https://doi.org/10.2307/2641229>.
- Zhang, Y., Mathur, R., Bash, J.O., Hogrefe, C., Xing, J., Roselle, S.J., 2018. Long-term trends in total inorganic nitrogen and sulfur deposition in the US from 1990 to 2010. *Atmos. Chem. Phys.* 18 (12), 9091–9106. <https://doi.org/10.5194/acp-18-9091-2018>.